Possible mechanism responsible for generating impurity outward flow under radio frequency heating

S. Moradi, T. Fülöp, A. Mollén, I. Pusztai

Department of Applied Physics, Nuclear Engineering, Chalmers University of Technology and Euratom-VR Association, Göteborg, Sweden

Abstract. The effect of poloidal asymmetry of impurities on impurity transport driven by electrostatic turbulence in tokamak plasmas is analyzed. It is found that in the presence of in-out asymmetric impurity populations the zero-flux impurity density gradient (the so-called peaking factor) is significantly reduced. A sign change in the impurity flux may occur if the asymmetry is sufficiently large. This may be a contributing reason for the observed outward convection of impurities in the presence of radio frequency heating. The present paper extends previous work [T. Fülöp and S. Moradi, *Phys. Plasmas* **18**, 030703 (2011)], by including the effect of ion parallel compressibility on the peaking factor, which is found to have a significant contribution in the presence of a poloidal asymmetry. It is shown here that in the ion temperature gradient mode dominated plasmas the presence of an in-out poloidal asymmetry can lead to negative impurity peaking factor, and it becomes more negative in regions with larger ion temperature gradients. In the trapped electron mode dominated plasmas an in-out poloidal asymmetry results in a strong reduction of the peaking factor, however, it remains positive for typical experimental parameters. Furthermore, it is shown that an up-down asymmetry reduces the peaking factor while an out-in asymmetry increases it.

PACS numbers: 52.25 Fi, 52.25 Ya, 52.55 Fa

1. Introduction

Accumulation of impurities in the core of fusion devices would have detrimental effect on fusion reactivity due to increased radiation losses and plasma dilution. Significant effort has therefore been spent during recent years to identify plasma conditions in which accumulation can be avoided. One of the most promising methods for obtaining flat or hollow impurity density profiles is to use radio frequency heating. This has been shown to work well in various experiments [1, 2, 3, 4, 5, 6, 7] but the physical mechanism by which the change of the direction of the impurity convective velocity occurs has not yet been clearly identified in spite of the various efforts that have been made [8, 9, 10]. In particular the reason for the flat impurity density profiles in ion cyclotron resonance heated (ICRH) discharges in JET has been debated for many years [1, 5, 6]. In a recent paper [11] it was shown that a poloidal asymmetry could lead to a significant reduction of the impurity zero-flux density gradient (also called the peaking factor), and even a sign change in the impurity flux, if the asymmetry is sufficiently large. Along with other effects, this may be a contributing factor to the avoidance of accumulation of high-Z impurities with ICRH. In this paper, we extend the analysis of Ref. [11], by including the effect of ion parallel compressibility on the peaking factor, and by presenting a numerical investigation of the effect of poloidal asymmetry on impurity transport. In particular, the dependence of the impurity density peaking factor on charge number, inverse ion- and electron temperature scale lengths and inverse electron density scale length is analyzed. The results are benchmarked to GYRO [12] in the poloidally symmetric case.

It is found that inboard accumulation gives rise to negative peaking factors (outward impurity convection and hollow impurity profile), in ion temperature gradient (ITG) mode driven turbulence, if the asymmetry is sufficiently large. Also in the trapped electron (TE) mode dominated case inboard accumulation results in a strong reduction of the peaking factor, however, it remains positive for typical experimental parameters. The sign and magnitude of the peaking factor will be shown to be sensitive not only to the asymmetry strength but also to the temperature gradient. As the ion temperature gradient increases in the ITG mode dominated case the impurity peaking factor becomes more negative. As noted in previous work [8], in the poloidally symmetric case, parallel compressibility has a significant effect on the peaking factor. As we will see in this paper this effect is also observed for asymmetric impurity densities, and leads to a peaking factor that is more sensitive to the ion temperature gradient than in the case without taking into account parallel compressibility.

The remainder of the paper is organized as follows. In Sec. 2 we describe the mechanism behind the impurity poloidal asymmetry that arises in the presence of ICRH. In Sec. 3 the model for calculating the quasilinear impurity flux and the peaking factor in the presence of poloidal asymmetry is presented. In Sec. 4 the parametric dependences of the peaking factor are analyzed by presenting scans over relevant parameters such as charge number, and temperature and density scale lengths. Also, the importance of the

impurity parallel compressibility is demonstrated. Finally, the results are discussed and summarized in Sec. 5.

2. Poloidal asymmetry

Poloidal impurity asymmetries in tokamaks can arise due to various reasons: e.g. difference in impurity source location, toroidal rotation or neoclassical effects. There is a wealth of experimental evidence for poloidal asymmetries [13, 14, 15, 16, 17, 18]. In the plasma core in-out asymmetries can arise due to the presence of radio frequency (RF) heating (henceforth "in-out" and "out-in" asymmetries will refer to the situations when the maximum of the poloidally varying impurity density is at the inboard and outboard sides of the plasma, respectively). A detailed physical explanation of why ICRH favors inboard accumulation, together with the description of the experimental results, is given in Ref. [13]. The RF-heating scheme applied in the experiment described in [13] is hydrogen-minority heating in a deuterium plasma. The underlying principle is that the asymmetry is a result of the increase of the hydrogen-minority density on the outboard side. These particles tend to be trapped on the outside of the torus and the turning points of their orbits drift towards the resonance layer due to the heating. The poloidal asymmetry in the hydrogen-minority density gives rise to an electric field that pushes the other ion species to the inboard side. In the case of highly-charged impurities, this effect is amplified by their higher charge Z.

The RF-induced accumulation of minority ions on the outboard side leads to a corresponding impurity accumulation on the inboard side by the following mechanism. If the plasma consists of electrons, bulk ions, impurity ions and RF-heated minority ions then it can be expected that all species except the minority ions are Boltzmann distributed (the dynamics of the minority ions is strongly affected by the heating). If a particle species a is Boltzmann distributed, the poloidal variation of the density is $\tilde{n}_a/n_{a0} \simeq -e_a\phi_E/T_a$, where the tilde denotes the variation on the flux surface, e_a is the charge and T_a is the temperature of the species. Quasineutrality requires that

$$n_{e0}\left(1+\frac{e\phi_E}{T_e}\right)-n_{D0}\left(1-\frac{e\phi_E}{T_i}\right)-n_{H0}\left(1-\frac{e\phi_E}{T_H}\right)-Zn_{Z0}\left(1-\frac{Ze\phi_E}{T_z}\right)=\hat{n}_H,$$

where the subscript zero indicates the density where the equilibrium potential ϕ_E vanishes, and $\hat{n}_H$ represents only the fraction of the hydrogen minority density which feels the ICRH resonance and does not follow Boltzmann ditribution. If ϕ_E is normalized so that $n_{D0}+n_{H0}+Zn_{Z0}-n_{e0}=0$, assuming similar temperature for the different ion species and $n_{H0} \ll n_{D0}$, the poloidal variation of the impurity density becomes

$$\frac{\tilde{n}_z}{n_{Z0}}=-\frac{Ze\phi_E}{T_z}=-\frac{Z\hat{n}_H/n_{D0}}{1+(T_i/T_e)+(n_{Z0}Z^2/n_{D0})}. \tag{1}$$

Since the poloidal variation in the impurity density has the opposite sign to that of the minority ions, the accumulation of the latter on the outboard side gives rise to an electric field that pushes the other ion species to the inboard side. Simulations of the

hydrogen ion distribution function in the presence of RF heating with the Monte Carlo code FIDO described in Ref. [13] show that a considerable out-in asymmetry in the hydrogen ion density can be expected, which is sufficient to account for the observed in-out asymmetry in the impurity density.

In the tokamak edge, where the plasma is sufficiently collisional, also steep radial pressure or temperature gradients can give rise to an in-out asymmetry. These effects have been observed in e.g. Alcator C-Mod [14], and it has been shown that the observations are in qualitative agreement with neoclassical theory [19, 20, 21, 22]. The sign and magnitude of these asymmetries depend sensitively and nonlinearly on magnetic geometry, fraction of impurities in the plasma and rotation. Neoclassical theory also predicts an up-down asymmetry, which is caused by the ion-impurity friction.

3. Impurity flux

Since impurity transport is usually dominated by drift-wave turbulence, in this work we focus on the effect of the impurity poloidal asymmetry on impurity transport driven by microinstabilities. We assume that the processes that cause the asymmetry are not affected significantly by the fact that the cross-field transport is dominated by fluctuations. For simplicity we consider only the collisionless, electrostatic case. The quasilinear impurity particle flux is given by

$$\Gamma_z = -\frac{k_\theta}{B}\mathrm{Im}\left[\hat{n}_z\phi^*\right], \tag{2}$$

where Im[·] denotes imaginary part, k_θ is the poloidal wave-number, $\hat{n}_z$ is the perturbed impurity density, ϕ^* is the complex conjugate of perturbed electrostatic potential ϕ.

The perturbed impurity density response in an axisymmetric, large aspect ratio torus with circular magnetic surfaces can be obtained from the linearized gyrokinetic equation, [23]

$$\frac{v_\parallel}{qR}\frac{\partial g_a}{\partial\theta} - i(\omega-\omega_{Da})g_a - C_a(g_a) = -i\frac{e_a f_{a0}}{T_a}\left(\omega-\omega_{*a}^T\right)\phi J_0(z_a), \tag{3}$$

where g_a is the nonadiabatic part of the perturbed distribution function, θ is the extended poloidal angle, $f_{a0} = n_a/\left(\sqrt{\pi}v_{Ta}\right)^3\exp(-x_a^2)$ is the equilibrium Maxwellian distribution function, $x_a = v/v_{Ta}$ is the velocity normalized to the thermal speed $v_{Ta} = (2T_a/m_a)^{1/2}$, n_a and m_a are the density and mass of species a, $\omega_{*a} = -k_\theta T_a/e_a B L_{na}$ is the diamagnetic frequency, $\omega_{*a}^T = \omega_{*a}\left[1+\left(x_a^2-\frac{3}{2}\right)L_{na}/L_{Ta}\right]$, $L_{na} = -[\partial(\ln n_a)/\partial r]^{-1}$, $L_{Ta} = -[\partial(\ln T_a)/\partial r]^{-1}$, are the density and temperature scale lengths, $\omega_{Da} = -k_\theta\left(v_\perp^2/2+v_\parallel^2\right)D(\theta)/\omega_{ca}R$ is the magnetic drift frequency, $D(\theta) = (\cos\theta + s\theta\sin\theta)$, $\omega_{ca} = e_aB/m_a$ is the cyclotron frequency, B is the equilibrium magnetic field, q is the safety factor, $s = (r/q)(dq/dr)$ is the magnetic shear, r and R are the minor and major radii, J_0 is the Bessel function of the first kind and $z_a = k_\perp v_\perp/\omega_{ca}$.

In the absence of collisions and in the limit $v_\parallel/qR(\omega-\omega_{Dz}) \ll 1$, Eq. (3) can be solved iteratively to find the non-adiabatic part of the perturbed impurity distribution.

Including the Boltzmann part of the distribution, the perturbed ion density response becomes [23, 24]

$$\frac{\hat{n}_z}{n_z} = -\frac{Ze\phi}{T_z} + \int d^3v \frac{ZeJ_0(z_z)}{n_z T_z}\left[1 - \frac{v_\parallel}{qR(\omega-\omega_{Dz})}\frac{\partial}{\partial\theta}\frac{v_\parallel}{qR(\omega-\omega_{Dz})}\frac{\partial}{\partial\theta}\right]\frac{\omega-\omega^T_{*z}}{\omega-\omega_{Dz}} f_{z0}J_0(z_z)\phi, \tag{4}$$

where parallel compressibility is represented by the term containing the two θ-derivatives.

The zero-flux impurity density gradient (the peaking factor) can be obtained from $\langle\Gamma_z\rangle = 0$ with the perturbed impurity density taken from (4). Here $\langle\cdots\rangle = (1/2\pi)\int_{-\pi}^{\pi}(\cdots)d\theta$. We model the poloidal asymmetry of the impurity density by the ansatz $n_z = n_{z0}\sum_n f_n \mathcal{P}(\theta,\delta,n)$, where $\mathcal{P}(\theta,\delta,n) = \left[\cos^2\left(\frac{\theta-\delta}{2}\right)\right]^n$, with δ representing the angular position where the impurity density has its maximum, n represents the peakedness of the asymmetry and the weights f_n can be chosen to represent populations of impurities with various degrees of peakedness. For evenly distributed impurity density $f_0 = 1$ and the rest of the weights $f_n = 0$ for $n \neq 0$. Figure 1 shows the asymmetry function $\mathcal{P}(\theta,\delta,n)$ as a function of normalized θ/π, for different values of the weights f_n. We note, that in general the impurity density cannot be factorized this way; which would mean a possible poloidal variation of the logarithmic density gradients. Nevertheless, to keep the theoretical treatment simple, we adopt the factorization, which is justified for cases where $d(d\ln n_Z/dr)/d\theta \ll d\ln n_Z/dr$. A similar asymmetry function was used also in previous work [11, 15].

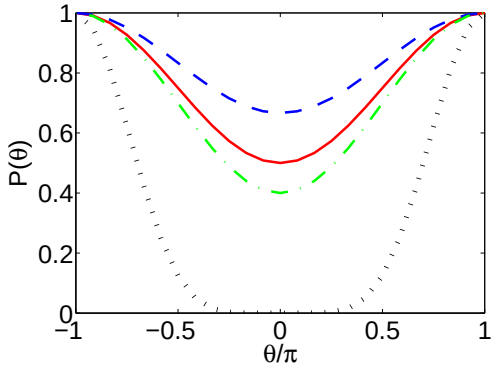

Figure 1. $\mathcal{P}(\theta,\pi,n)$ as a function of normalized θ/π, for different values of f_n. Solid line (red) represents $f_0 = f_1 = 1$, dashed line (blue) is for $f_0 = 1, f_1 = 0.5$, dash-dotted line (green) is for $f_0 = f_1 = 1$ and $f_2 = 0.5$, dotted line (black) is for $f_3 = 1$. The rest of the f_ns are assumed to be zero.

The impurity flux can be calculated numerically, by solving the velocity-space integrals in the perturbed impurity density (4) in the expression for the impurity flux (2), without the constant energy resonance approximation $[v_\perp^2 + 2v_\parallel^2 \to 4(v_\perp^2 + v_\parallel^2)/3]$ [23] or the assumption on the smallness of the finite Larmor radius parameter. These approximations were used in Ref. [11].

The impurity peaking factor a/L_{nz}^0 can be obtained by setting the impurity flux to zero, or $\langle \mathrm{Im}[\hat{n}_z \phi^*] \rangle = 0$. Here, the fluctuating density is given by Eq. (4), a is the outermost minor radius, and a/L_{nz}^0 is calculated as

$$a/L_{nz}^0 = \frac{\langle \mathrm{Im}[S_T(\theta)\phi^*] \rangle}{\langle \mathrm{Im}[S_n(\theta)\phi^*] \rangle}, \tag{5}$$

where

$$S_n(\theta) = \int d^3x_z e^{-x_z^2} J_0[z_z(\theta)] \left(1 - \delta_p \mathcal{M}_\theta\right) \frac{\bar{\omega}_{*z} \mathcal{P}(\theta) \phi(\theta) J_0[z_z(\theta)]}{\bar{\omega} - \bar{\omega}_{Dz}(\theta)}, \tag{6}$$

and

$$S_T(\theta) = \int d^3x_z e^{-x_z^2} J_0[z_z(\theta)] \left(1 - \delta_p \mathcal{M}_\theta\right) \frac{[\bar{\omega} - \bar{\omega}_{*z}(x_z^2 - 3/2)a/L_{Tz}] \mathcal{P}(\theta) \phi(\theta) J_0[z_z(\theta)]}{\bar{\omega} - \bar{\omega}_{Dz}(\theta)}, \tag{7}$$

with the operator representing parallel compressibility

$$\mathcal{M}_\theta = \frac{x_{z\|}}{R(\theta)(\bar{\omega} - \bar{\omega}_{Dz}(\theta))} \frac{\partial}{\partial \theta} \frac{x_{z\|}}{R(\theta)(\bar{\omega} - \bar{\omega}_{Dz}(\theta))} \frac{\partial}{\partial \theta}, \tag{8}$$

where $R(\theta) = R_0(1 + \epsilon \cos\theta)$ with $\epsilon = r/R_0$, $\delta_p = 2a^2 m_i/(q^2 m_z \tau_z)$, $\tau_z = T_e/T_z$, $b = (\rho_s/Z)\sqrt{2A_Z/\tau_z A_i}$, ρ_s is the ion sound Larmor radius, $\bar{\omega}_{*z} = -k_\theta \rho_s/Z\tau_z$, $\bar{\omega}_{Dz} = -2k_\theta \rho_s (a/R)(x_{z\perp}^2/2 + x_{z\|}^2) D(\theta)/Z\tau_z$, $z_z(\theta) = x_{z\perp} b k_\perp(\theta)$, and $k_\perp = k_\theta \sqrt{1 + s^2\theta^2}$. All frequencies marked with bars are in c_s/a units, where c_s is the ion sound speed, and the main ion and impurity temperature gradients are assumed to be equal $a/L_{Tz} = a/L_{Ti}$.

4. Parametric dependences of the peaking factor

In the calculations presented in this section we have used the following local profile and magnetic geometry parameters: $r/a = 0.3$, $R/a = 3$, $k_\theta \rho_s = 0.3$, $q = 1.7$, $a/L_{ne} = 1.5$, $T_i/T_e = 0.85$, $a/L_{Te} = 2$, $a/L_{Ti} = 2.5$, $s = 0.22$ and $\rho_s/a = 0.0035$. This is the baseline case in our study, and these parameters will be used unless otherwise stated. The impurities are assumed to be present in trace quantities, in the sense that $Zn_z/n_e \ll 1$ ($n_z/n_e = 2 \times 10^{-3}$ is used in the simulations). To study the effect of the strength of the asymmetry we present results for $n = 0$ to $n = 3$, and assume $f_j = 1$ for the specific asymmetry strength (for instance if $n = 3$ we use $f_3 = 1$ and $f_j = 0$ for $j \neq 3$).

The perturbed electrostatic potential and eigenvalues (which are practically unaffected by the presence of a poloidally asymmetric *trace* impurity species) have been obtained by linear electrostatic gyrokinetic calculations with GYRO. We note that the electron and main ion densities are assumed to be approximately poloidally symmetric. This is important for our model to be valid, since GYRO assumes poloidally symmetric background plasma parameters. We would like to emphasize, that – as it can be seen from Eqs. (5-7) – the zero flux impurity density gradient does not depend on any constant multiplier of the perturbed potential.

4.1. Charge number dependence

The peaking factor as a function of charge number for various impurity poloidal asymmetries is shown in Fig. 2. In the poloidally symmetric case (solid line in Fig. 2a), the peaking factor is not sensitive to the charge number, as has been noted before, in both fluid and gyrokinetic simulations of ITG turbulence dominated transport, without taking into account the poloidal impurity asymmetries [8, 25]. The situation is similar also in case of up-down asymmetric impurity populations or outboard accumulation. Out-in asymmetry gives slightly higher and up-down asymmetry gives lower peaking factors. However, in agreement with the conclusion of [11], impurities experience outward convection (corresponding to negative peaking factor) if the impurity density is accumulated on the inboard side, as it is shown with the black dotted line in Fig. 2a. The change in the peaking factor becomes stronger as the asymmetry is increased, as it is illustrated in Fig. 2b. Note, that the strength of the asymmetry is also expected to depend on Z, and usually it is larger for heavy impurities, as it was shown in Sec. 2. According to Eq. (1), in the limit of trace impurities, the poloidal variation of the impurity density is proportional to the charge number.

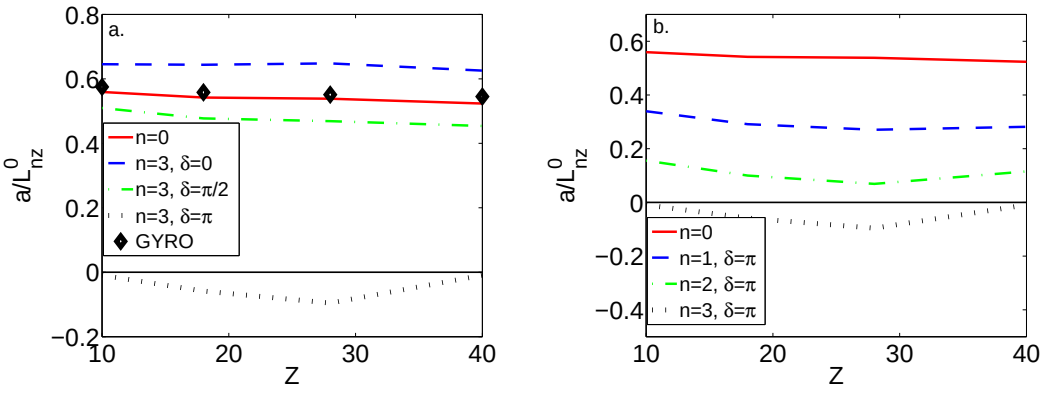

Figure 2. Peaking factor as a function of charge number for different values of peaking angle δ (a) and asymmetry strength n (b). The rest of the parameters are taken from the baseline case, for which the eigenvalue is $\omega = (-0.0224 + i\ 0.225)c_s/a$. In both figures the solid line represents the case of poloidally symmetric impurity distribution. (a): $n = 3$ – out-in asymmetry (blue, dashed), up-down asymmetry (green, dash-dotted), in-out asymmetry (black, dotted). (b): in-out asymmetry – $n = 1$ (blue, dashed), $n = 2$ (green, dash-dotted), $n = 3$ (black, dotted).

In order to examine the importance of parallel compressibility in determining the charge dependence of the impurity peaking factor we separate the terms independent and proportional to δ_p (representing the parallel compressibility) in Eq. (6) as $S_n(\theta) = S_n^1(\theta) + S_n^{pc}(\theta)$, where

$$S_n^1(\theta) = \mathcal{P}(\theta)\phi(\theta) \int d^3x_z e^{-x_z^2} J_0^2[z_z(\theta)] \frac{\bar{\omega}_{*z}}{\bar{\omega} - \bar{\omega}_{Dz}(\theta)}, \tag{9}$$

$$S_n^{pc}(\theta) = -\delta_p \int d^3x_z e^{-x_z^2} J_0[z_z(\theta)] \mathcal{M}_\theta \frac{\bar{\omega}_{*z} \mathcal{P}(\theta)\phi(\theta) J_0[z_z(\theta)]}{\bar{\omega} - \bar{\omega}_{Dz}(\theta)}, \tag{10}$$

and in Eq. (7) as $S_T(\theta) = S_T^1(\theta) + S_T^{pc}(\theta)$, where

$$S_T^1(\theta) = \mathcal{P}(\theta)\phi(\theta) \int d^3x_z e^{-x_z^2} J_0^2[z_z(\theta)] \frac{\bar{\omega} - \bar{\omega}_{*z}(x_z^2 - 3/2)a/L_{Tz}}{\bar{\omega} - \bar{\omega}_{Dz}(\theta)}, \tag{11}$$

$$S_T^{pc}(\theta) = -\delta_p \int d^3x_z e^{-x_z^2} J_0[z_z(\theta)] \mathcal{M}_\theta \frac{[\bar{\omega} - \bar{\omega}_{*z}(x_z^2 - 3/2)a/L_{Tz}]\mathcal{P}(\theta)\phi(\theta) J_0[z_z(\theta)]}{\bar{\omega} - \bar{\omega}_{Dz}(\theta)}. \tag{12}$$

Using the above notations the peaking factor can be rewritten as:

$$a/L_{nz}^0 = \frac{\langle \mathrm{Im}[S_T^1(\theta)\phi^*] \rangle + \langle \mathrm{Im}[S_T^{pc}(\theta)\phi^*] \rangle}{\langle \mathrm{Im}[S_n^1(\theta)\phi^*] \rangle + \langle \mathrm{Im}[S_n^{pc}(\theta)\phi^*] \rangle}. \tag{13}$$

Figure 3 shows these four expressions as functions of impurity charge for the symmetric and in-out asymmetric cases with an asymmetry strength of $n = 3$. In the denominator, the terms independent of δ_p, i.e. $S_n^1(\theta)$, are the dominant contributors in both the symmetric and asymmetric cases. These are proportional to $1/Z$. But in the numerator, the balance between the terms proportional and independent of δ_p is very different between the symmetric and asymmetric cases; in the symmetric case $S_T^1(\theta)$ is the dominant term, while in the asymmetric case $S_T^{pc}(\theta)$ is dominant. These results show that if an in-out asymmetry is present, the parallel compressibility effects become more important than the other terms, and therefore, have to be taken into account.

In the following we will concentrate on the peaking factor for nickel which was one of the impurities studied in Ref. [1]. Figure 4 shows the peaking factor for nickel for various accumulation maxima δ and asymmetry strengths n. The peaking factor increases slightly for out-in accumulation but the more dramatic change – including a sign-change – is expected only for inboard accumulation. The sign change occurs when $n \simeq 2.5$. In Ref. [11] it was shown that without taking into account the effect of parallel compressibility the sign change occurs when $n \simeq 3$. This is in agreement with the results obtained here if parallel compressibility effects are neglected, i.e. by setting $\delta_p = 0$ in Eqs. (6) and (7) (as will be shown later in Fig. 12).

4.2. Temperature gradient dependence

The eigenvalues and electrostatic potentials as functions of ion- and electron temperature gradients are shown in Figs. 5-6. As expected, if we increase the ion temperature gradient, the turbulence becomes more ITG-dominated (the real part of the mode frequency ω_r is negative), while if we increase the electron temperature gradient, TE-mode driven turbulence will dominate (ω_r is positive). The shape of the imaginary part of the potential $\mathrm{Im}[\phi]$ varies slightly by increasing the temperature gradient for both the ITG and TE-mode dominated cases, while the real parts of the potential $\mathrm{Re}[\phi]$ are not modified significantly, see Fig. 6. The imaginary part of the potential plays an important role in the parallel compressibility terms and therefore the change in the temperature gradient will modify the impurity peaking factor.

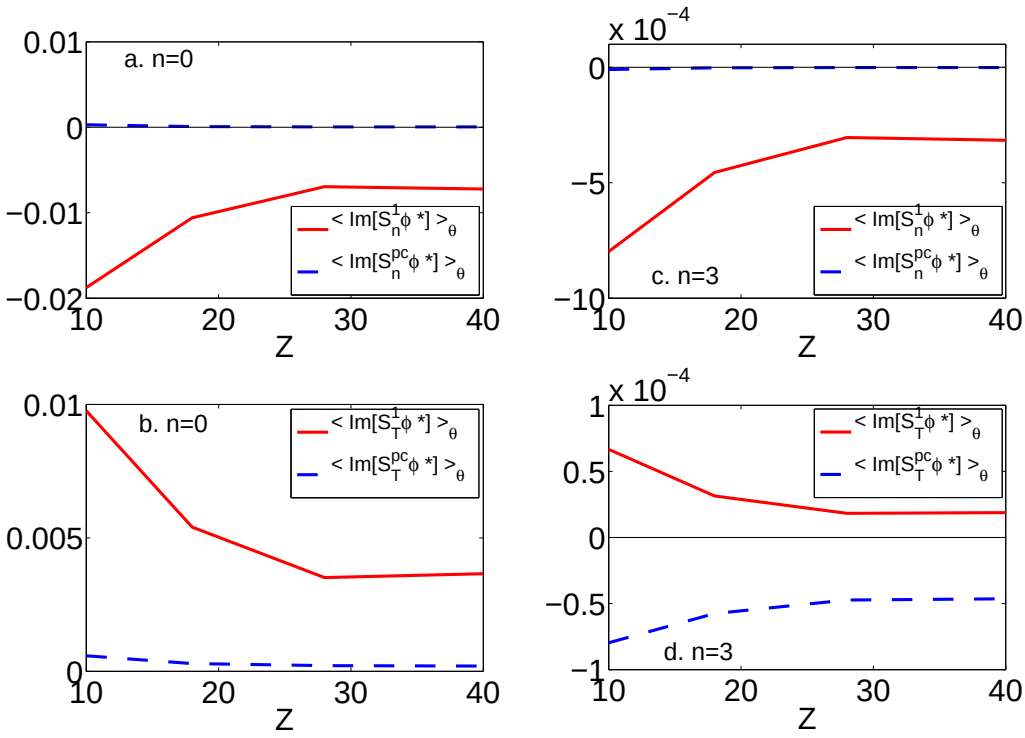

Figure 3. Terms proportional (dashed lines) and independent of δ_p (solid lines) in Eq. (13) as functions of impurity charge Z. (a) and (c) show the terms in the denominator and (b) and (d) show the terms in the numerator. (a) and (b) correspond to the poloidally symmetric case, and (c) and (d) correspond to in-out asymmetry with strength $n = 3$.

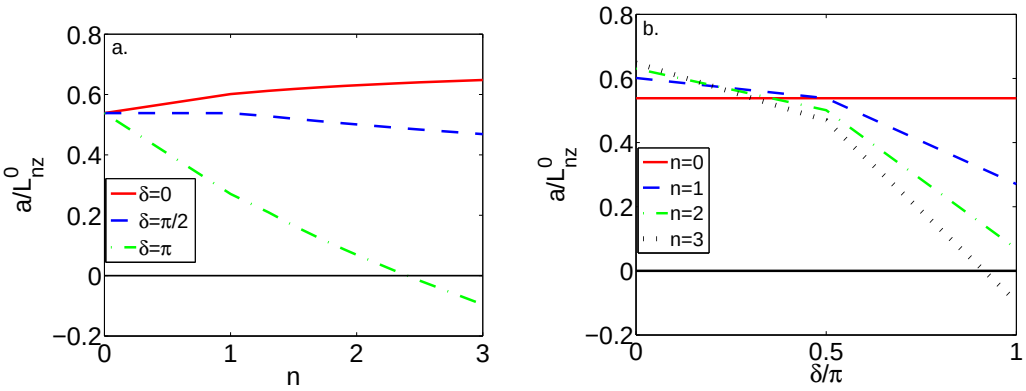

Figure 4. Peaking factor for nickel as a function of n (a) and δ (b). (a): symmetric impurity density (solid, red), up-down asymmetry (dashed, blue), and in-out asymmetry (dash-dotted, green). (b): symmetric impurity density (solid, red), $n = 1$ (dashed, blue), $n = 2$ (dash-dotted, green), and $n = 3$ (dotted, black).

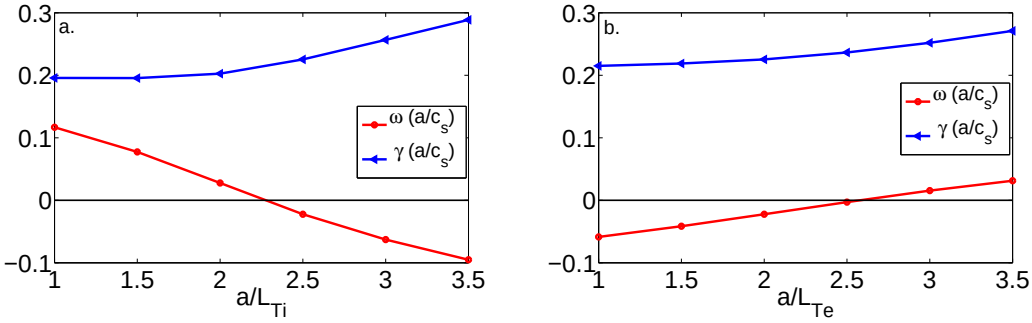

Figure 5. Real and imaginary parts of $\omega = \omega_r + i\gamma$ as function of a/L_{Ti} (a) and a/L_{Te} (b) obtained by GYRO for the baseline case. Blue lines (with circle markers) represent the real part, blue lines (triangle markers) correspond to the imaginary part of the eigenvalue. The frequencies are normalized to c_s/a.

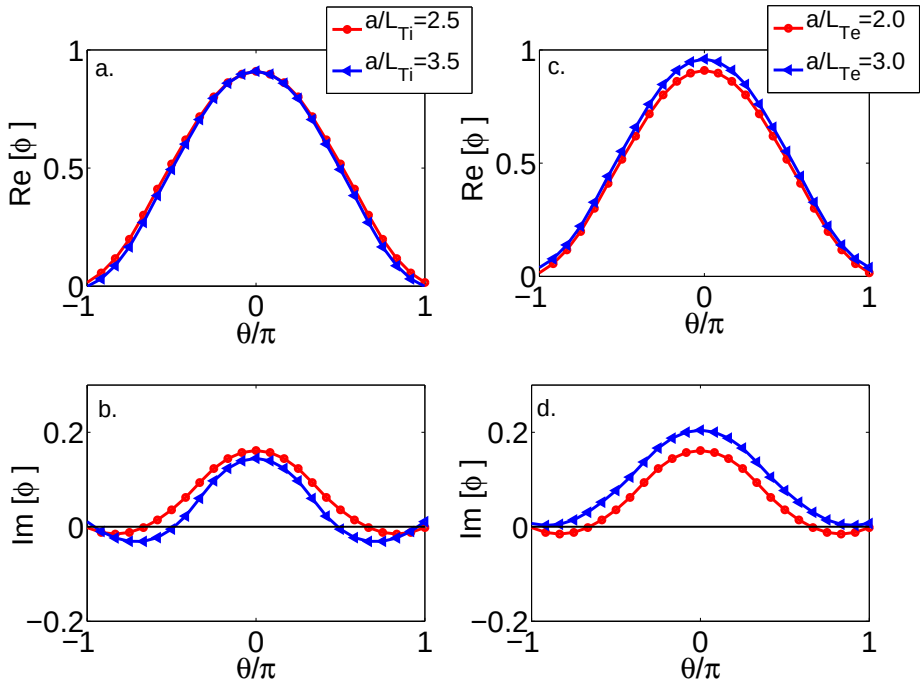

Figure 6. Real and imaginary parts of the electrostatic potentials in the cases corresponding to Fig. 5 for different ion- (a,b) and electron (c,d) temperature gradients. (a) and (c) show the real parts and (b) and (d) show the imaginary parts of ϕ (note the different scale). Red lines (circle markers) show the temperature gradient corresponding to the baseline case and blue lines (triangle markers) show the case with the larger temperature gradient.

Previous works highlighted the difference in peaking factors between ITG and TE dominated cases, and concluded that ITG-dominated turbulence will always generate inward pinch of impurities, while in TE-mode driven turbulence outward convection in the plasma core (for $r/a \simeq 0.2$) can be expected. Both linear [7, 8] and non-linear [26] gyrokinetic simulations have shown that the latter is due to the contribution from the parallel dynamics which can reverse the impurity convection from inwards to outwards for modes propagating in the electron direction. These results are in agreement, under some conditions, with the experimental observation that the impurity convection changes sign from inward to outward when a strong central peaking of the electron temperature arises as a response to strong localized central electron heating. However, these results cannot explain the outward convection of impurities observed in experiments with RF heating where the ITG-mode is the dominant instability.

Our results show, that the peaking factor can become negative in the ITG-dominated case if the impurities accumulate on the inboard side, and it is influenced very strongly by increasing temperature gradients.

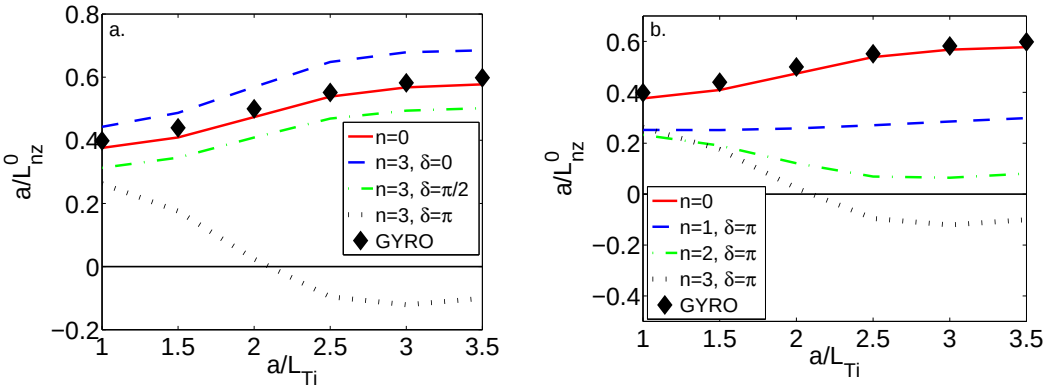

Figure 7. Peaking factor for nickel as a function of ion temperature gradient for different values of δ (a) and n (b). In both figures the solid line represents the case of poloidally symmetric impurity distribution; in figure (a) this case is compared to GYRO simulations (black diamonds). (a): $n = 3$ – out-in asymmetry (dashed), up-down asymmetry (dash-dotted), in-out asymmetry (dotted). (b): in-out asymmetry – $n = 1$ (dashed, blue), $n = 2$ (dash-dotted, green), $n = 3$ (dotted, black).

Figure 7 shows the ion temperature-gradient scaling of the peaking factor and the diamond symbols show these values obtained by GYRO simulations in the poloidally symmetric limit, which present good agreement with our results. The peaking factor increases with the ion temperature gradient as long as the impurity density is poloidally symmetric or if it is up-down or out-in asymmetric. However, if the impurity density is in-out asymmetric then the sign of the peaking factor is negative for large temperature gradients, if the asymmetry is sufficiently large. The threshold for the sign change for the experimental scenario studied in this paper is $a/L_{Ti} \simeq 2$. As the strength of the asymmetry, n, is increased for an in-out asymmetry the modifications of the peaking

factor become stronger, see Fig. 7b.

As the electron temperature gradient is increased the turbulence becomes more TE dominated. Figure 8 shows that the absolute value of the peaking factor is strongly reduced in magnitude in the presence of an in-out asymmetry, however, it remains positive. Stronger asymmetries are needed in the TE dominated case in order to obtain a sign change.

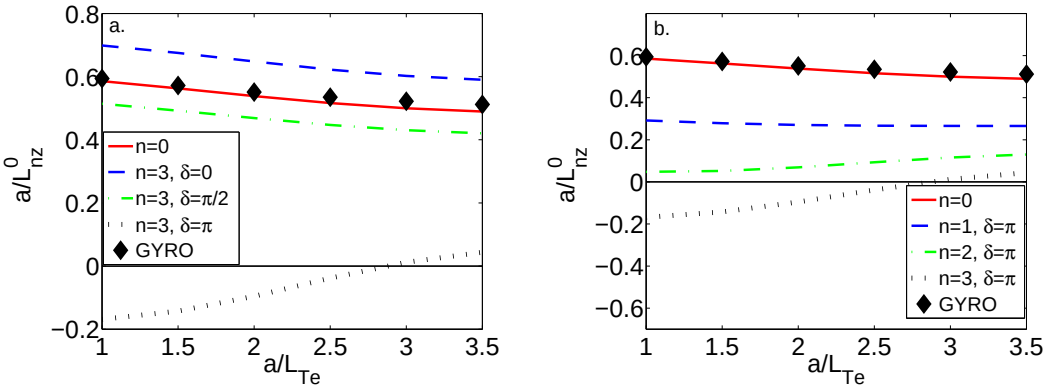

Figure 8. Peaking factor for nickel as a function of electron temperature gradient for different values of δ (a) and n (b). In both figures the solid line represents the case of poloidally symmetric impurity distribution; in figure (a) this case is compared to GYRO simulations (black diamonds). (a): $n = 3$ – out-in asymmetry (dashed, blue), up-down asymmetry (dash-dotted, green), in-out asymmetry (dotted, black). (b): in-out asymmetry – $n = 1$ (dashed, blue), $n = 2$ (dash-dotted, green), $n = 3$ (dotted, black).

4.3. Density gradient dependence

The density gradient scaling of the peaking factor is shown in Fig. 9. As the density gradient is increased the underlying instability changes from ITG- to TE-mode, see Fig. 10. The peaking factor is slightly decreasing with electron density gradient in the case of poloidal symmetry and in the cases of up-down or out-in asymmetries. Also here, the in-out asymmetric impurity density leads to negative peaking factor if the strength of the asymmetry is sufficient. It is interesting to note, that in the case of in-out asymmetry the peaking factor is quite sensitive to the density gradient. The difference between the two cases $a/L_{ne} = 0.5$ and $a/L_{ne} = 1.5$ can be understood by comparing the shape of the imaginary part of the electrostatic potential Im$[\phi]$ in Fig. 11b. It can be noted that by changing the density gradient, Im$[\phi]$ changes significantly. Note that it is mainly the part of the potential which is close to $\theta = \pi$ which is important, and it is considerably different for the two density gradients shown in Fig. 11b and therefore also the result for the peaking factor changes dramatically. Even though for $a/L_{ne} = 0.5$ the ITG mode is the dominant instability the peaking factor remains positive even for strong in-out asymmetries. This is different from the ITG-dominated cases in the previous

two subsections where the peaking factors were negative in the presence of an in-out asymmetry with the same strength. The difference in the electrostatic potentials is the underlying reason for the difference in the trends seen in Figs. 7-9.

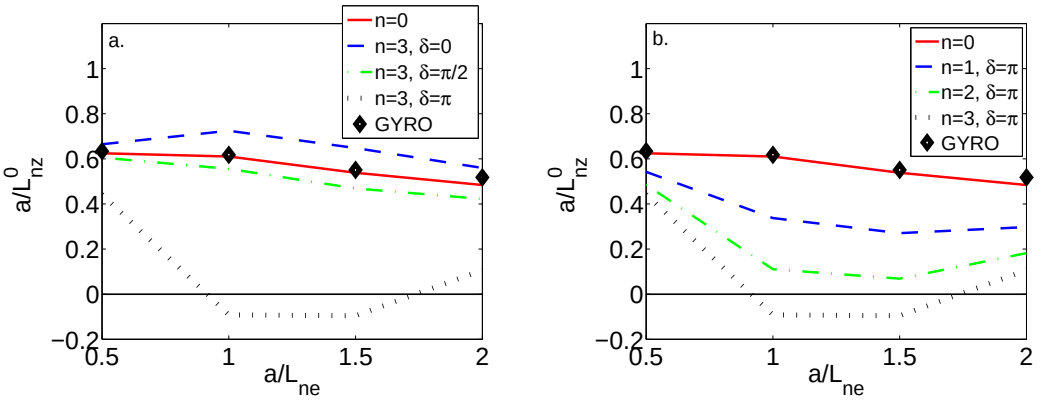

Figure 9. Peaking factor for nickel as a function of electron density gradient for different values of δ (a) and n (b). In both figures the solid line represents the case of poloidally symmetric impurity distribution; in figure (a) this case is compared to GYRO simulations (black diamonds). (a): $n = 3$ – out-in asymmetry (dashed, blue), up-down asymmetry (dash-dotted, green), in-out asymmetry (dotted, black). (b): in-out asymmetry – $n = 1$ (dashed, blue), $n = 2$ (dash-dotted, green), $n = 3$ (dotted, black).

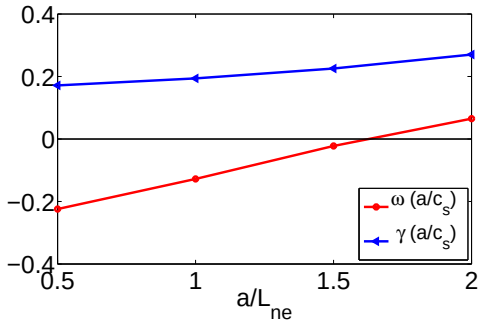

Figure 10. Real and imaginary parts of the eigenvalues as function of a/L_{ne} obtained by GYRO. Red lines (with circle markers) represent the real part, blue lines (triangle markers) correspond to the imaginary part of the eigenvalue. The frequencies are normalized to c_s/a.

4.4. Effect of parallel compressibility

It has been shown previously that when the transport is TE-mode dominated parallel compressibility effects generate an outward contribution to impurity anomalous flux which can, under certain plasma conditions, cancel out the inward contributions, leading to zero or even negative impurity peaking factor [7, 8]. In this subsection, we examine

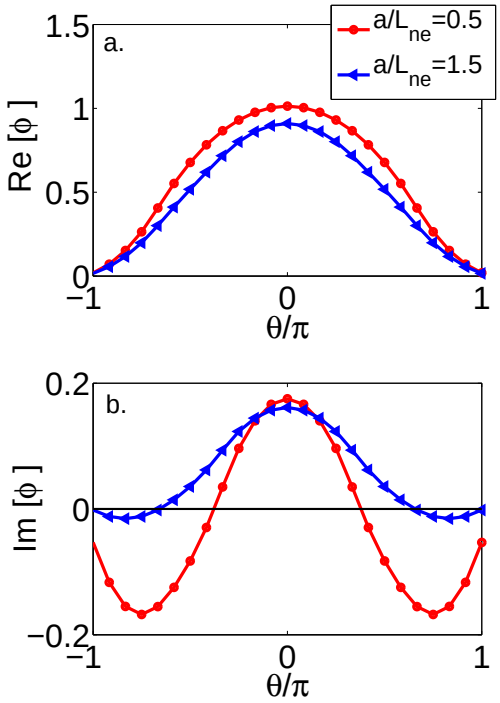

Figure 11. Real- (a) and imaginary (b) parts of the electrostatic potentials for two different density gradients.

this effect by neglecting the parallel compressibility terms, i.e. terms proportional to δ_p in Eqs. (6) and (7). Note that in this case only the absolute value of the potential enters in the expressions, while in the case with parallel compressibility both the imaginary and real parts and their derivatives are important.

Figure 12 shows the peaking factor for various δ and n. The effect of poloidal asymmetry in this limit is in agreement with our previous work in Ref. [11] and is similar to that in the previous sections where the parallel compressibility effects are considered. As seen in Fig. 12a, in the absence of parallel compressibility effects an in-out asymmetry can lead to a negative peaking factor (outward impurity flux). An increase of the poloidal in-out asymmetry will increase the outward flux of impurities as shown in Fig. 12b. Note that in the case with parallel compressibility, the sign change in the peaking factor occurs for broader range of δ and for lower asymmetry strength (compare Figs. 4 and 12). Also an up-down asymmetry can lead to a slight reduction of the impurity peaking factor. This is similar to the case where the parallel compressibility was taken into account, see Fig. 4a.

Figure 13 shows the ion temperature-gradient scan for the peaking factor without parallel compressibility. The diamonds represent the values of the peaking factor obtained by GYRO (without parallel compressibility) which show agreement with our results in the symmetric limit. From Fig. 13 it is clear that without parallel compressibility the peaking factor is less sensitive to the increase of the ion temperature

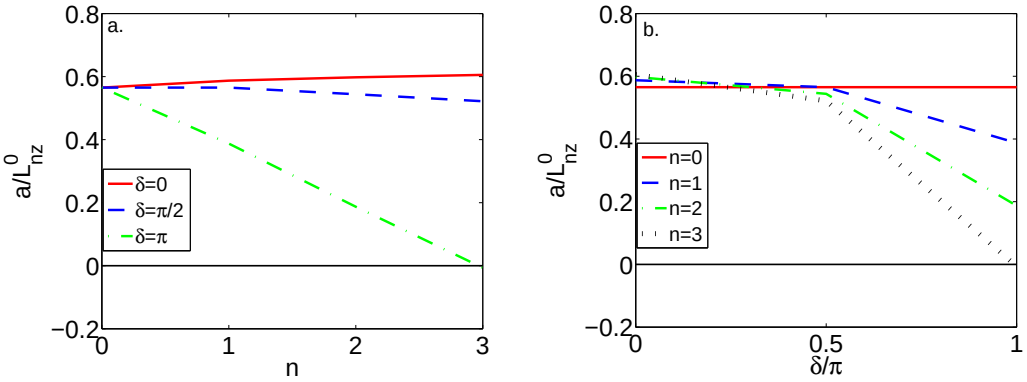

Figure 12. Peaking factor for nickel as a function of n (a) and δ (b), without taking into account parallel compressibility. (a): symmetric impurity density (solid, red), up-down asymmetry (dashed, blue), and in-out asymmetry (dash-dotted, green). (b): in-out asymmetry – symmetric impurity density (solid, red), $n = 1$ (dashed, blue), $n = 2$ (dash-dotted, green) and $n = 3$ (dotted, black).

gradient, and in the presence of an asymmetry, regardless of the asymmetry sign, when the transport is TE-mode dominated the peaking factor remains positive. In the ITG mode dominated case, including effects of parallel compressibility the in-out asymmetry results in significantly larger negative peaking factors than without, compare Fig. 13 to Fig. 7a.

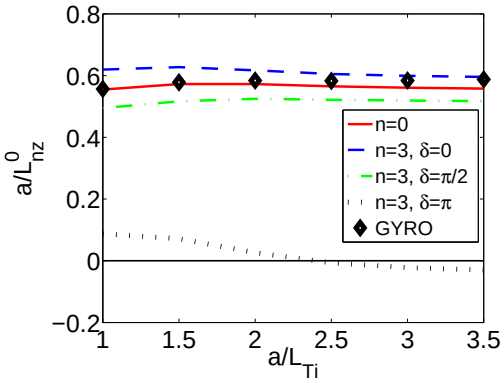

Figure 13. Peaking factor for nickel as a function of ion temperature gradient for different values of δ, without taking into account parallel compressibility. Solid (red) line represents the case of poloidally symmetric impurity distribution; in figures (a-c) this is compared to GYRO simulations (black diamonds). Out-in asymmetry (dashed, blue) up-down asymmetry (dash-dotted, green), in-out asymmetry (dotted, black).

5. Discussion and conclusions

For tokamak operation the avoidance of central impurity accumulation is a key issue. Conditions in which the convective impurity flux is directed outward are particularly interesting. In order to find such conditions many experiments have been devoted to explore various techniques. One way to expel the impurities from the plasma core is to maintain sawtooth crashes in a controlled way by applying central ICRH [27, 28]. It is observed that this method will indeed remove the impurities from the plasma core. However, it was shown that even though sawtooth crashes hamper the accumulation of the impurities their contribution is less relevant compared to the effect of the ICRH itself [5]. Another technique which has been successful in removing the impurities from the plasma core and is routinely used in tokamak experiments such as in the ASDEX-U tokamak is the application of a very localized central ECRH [29]. Simulations with both linear and non-linear gyrokinetic models have shown that under these conditions the electron temperature gradient is strongly peaked and therefore, modes propagating in the electron diamagnetic drift direction are the dominant instability responsible for the turbulence driven transport [26]. The interaction between the related electrostatic potential fluctuations and the parallel dynamics of the impurities leads to an outward convection of impurities. These results are in agreement with experimental observation in ASDEX-U for the very central region ($r/a \simeq 0.2$) [7]. In other tokamak experiments for example at JET the application of the central RF heating has also been explored with success. In these experiments it has been observed that the dominant instabilities are not TE-modes but rather modes directed in the ion diamagnetic drift direction, ITG-modes, which theoretically should result in an inward impurity flux. It has been debated that in the very central region of plasmas at JET the transport is mostly driven by neoclassical effects. By applying a strong central heating as the temperature gradient peaks the neoclassical temperature screening effects become dominant and result in an outward directed impurity flux. Under some plasma conditions these effects may be the reason for the observed behavior [2] however, usually the observed transport is an order of magnitude larger than the neoclassical predictions implying that the impurity transport is turbulence driven [26].

In the present work we discuss the impact of poloidal dependence of the impurity density on the impurity peaking factor in the core of tokamak plasmas. Various mechanisms may give rise to a poloidal asymmetry of impurity density: difference in impurity source location, toroidal rotation or neoclassical effects. Among these is an in-out poloidal asymmetry observed in plasmas where RF heating is applied. The mechanism responsible for this behavior was explained through RF-induced accumulation of minority ions on the outboard side of the torus giving rise to a corresponding impurity accumulation on the inboard side as was discussed in Ref. [13] and in Sec. 2. The strength of the impurity accumulation depends on the impurity charge (higher for heavier impurities) and the plasma parameters such as temperature gradient. However, the exact form of these dependences is not yet known and further

analysis is needed in this area. It is out of the scope of the present paper to make an extensive analysis of the above mentioned phenomena; the main objective of the paper is to demonstrate theoretically, assuming a simple ansatz for the poloidal asymmetry of impurity density, what effect it would have on the impurity transport.

In the parameter scans, for simplicity, we only presented the asymmetry function $\mathcal{P}(\theta, \delta, n)$ for a specific asymmetry strength, with weight $f_j = 1$. The total peaking factor can be estimated from the sum of the various peaking factors weighted in an appropriate way. For instance, for an asymmetric population, such that $n_z = n_{z0} + n_{z1}$ with $\langle n_{z0} \rangle / \langle n_{z1} \rangle = f_0/f_1$ (and $f_j = 0$ for $j \neq 0, 1$) the peaking factor can be estimated to be

$$\frac{a}{L_{nz}^0} \simeq \frac{a}{\langle n_0 + n_1 \rangle} \frac{\partial \langle n_0 + n_1 \rangle}{\partial r} \simeq \frac{f_0}{f_0 + f_1} \frac{a}{L_{nz0}} + \frac{f_1}{f_0 + f_1} \frac{a}{L_{nz1}}$$

where a/L_{nz0} is the peaking factor corresponding to the the poloidally symmetric part ($n = 0$, with weight f_0), and a/L_{nz1} is the peaking factor corresponding to the poloidally asymmetric part ($n = 1$, with weight f_1).

We have found that an in-out poloidal asymmetry of the impurity density ($\delta = \pi$) can lead to an outward impurity flux (negative peaking factor) in both ITG and TE mode dominated cases, and this effect becomes stronger as the asymmetry strength (n) increases. However, stronger asymmetries are needed in the TE mode dominated case in order to obtain a sign change. The level of asymmetry that is needed to change the sign of the peaking factor is too large in order for this effect alone to explain the observed outward convection. The RF-induced asymmetry can give rise to a poloidal variation of the order of 10-20% and that is much smaller than what is necessary for a sign change. However, together with other effects (e.g. neoclassical temperature screening, sawteeth) poloidal asymmetries can also contribute to the avoidance of central accumulation of impurities. The sign and magnitude of the peaking factor is sensitive not only to the asymmetry strength but also to the temperature gradient. In the ITG mode dominated case the in-out asymmetry results in a more negative peaking factor as the ion temperature gradient increases while in the TE mode dominated case as the electron temperature increases the peaking factor becomes more positive.

Our results indicate that an out-in asymmetry leads to an increase of the peaking factor, as it is observed in the NBI heated plasmas where the out-in asymmetry is generated by the centrifugal force on the impurity ions. It is also shown that an up-down asymmetry can lead to a reduction of the peaking factor. This can be a contributing reason for the observed flat impurity density profiles in plasmas with ECRH, and up-down asymmetries have indeed been observed in EC heated plasmas [15], although the physical mechanism for these asymmetries is not entirely understood.

The reason for the sign change of the impurity peaking factor in the presence of a poloidal asymmetry is attributed to the interaction between the poloidal variation of the related electrostatic potential and the poloidal dependence of the impurity density. If parallel compressibility effects are taken into account the imaginary part of the electrostatic potential is the determining factor in the sign change of the impurity

peaking factor.

In summary, our results suggest that poloidal asymmetries can significantly alter the turbulence driven impurity transport and therefore, have to be taken into account. These asymmetries may have a significant role in determining the impurity accumulation properties in plasmas with radio frequency heating. Therefore, there is a strong need for development of new tools in order to detect poloidal asymmetries and determine the effect of RF heating in their generation and the dependence of the asymmetry function to various plasma parameters.

Acknowledgments

The authors would like to thank J Candy for providing the GYRO code. This work was funded by the European Communities under Association Contract between EURATOM and *Vetenskapsrådet*. The views and opinions expressed herein do not necessarily reflect those of the European Commission.

Reference

[1] M. Valisa, L. Carraro, I. Predebon, M.E. Puiatti, C. Angioni, I. Coffey, C. Giroud, L. Lauro Taroni, B. Alper, M. Baruzzo, P. Belo daSilva, P. Buratti, L. Garzotti, D. Van Eester, E. Lerche, P. Mantica, V. Naulin, T. Tala, M. Tsalas and JET-EFDA contributors, *Nucl. Fusion*, **51** 033002 (2011).

[2] R. Dux, R. Neu, A. G. Peeters, G. Pereverzev, A. Muck, F. Ryter, J. Stober and ASDEX Upgrade Team, *Plasma Phys. Control. Fusion*, **45** 1815 (2003).

[3] R. Dux, C. Giroud, R. Neu, A.G. Peeters, J. Stober, K.-D. Zastrow, Contributors to the EFDA-JET Workprogramme, ASDEX Upgrade Team, *Journal of Nucl. Materials*, **313-316** 1150 (2003).

[4] R. Neu, R. Dux, A. Geier, H. Greuner, K. Krieger, H. Maier, R. Pugno, V. Rohde, S.W. Yoon, ASDEX Upgrade Team, *Journal of Nucl. Materials* ,**313-316**, 116 (2006).

[5] M. E. Puiatti, M. Valisa, M. Mattioli, T. Bolzonella, A. Bortolon, I. Coffey, R. Dux, M. von Hellermann, P. Monier-Garbet, M. F. F. Nave, J. Ongena and contributors to the EFDA-JET Workprogramme, *Plasma Phys. Control. Fusion*, **45** 2011 (2003).

[6] M. E. Puiatti, M. Valisa, C. Angioni, L. Garzotti, P. Mantica, M. Mattioli, L. Carraro, I. Coffey, C. Sozzi and JET-EFDA contributors, *Phys. Plasmas*, **13** 042501 (2006).

[7] C. Angioni, L. Carraro, T. Dannert, N. Dubuit, R. Dux, C. Fuchs, X. Garbet, L. Garzotti, C. Giroud, R. Guirlet, F. Jenko, O. J. W. F. Kardaun, L. Lauro-Taroni, P. Mantica, M. Maslov, V. Naulin, R. Neu, A. G. Peeters, G. Pereverzev, M. E. Puiatti, T. Pütterich, J. Stober, M. Valovic, M. Valisa, H. Weisen, A. Zabolotsky, ASDEX Upgrade Team, and JET EFDA Contributors, *Phys. of Plasmas* **14** 055905 (2007).

[8] C. Angioni and A. G. Peeters, *Phys. Rev. Lett.* **96**, 095003 (2006).

[9] C. Angioni, R. Dux, E. Fable, A. G. Peeters and the ASDEX Upgrade Team, *Plasma Phys. Control. Fusion*, **49** 2027 (2007).

[10] H. Nordman, R. Singh, T. Fülöp, L.-G. Eriksson, R. Dumont, J. Anderson, P. Kaw, P. Strand, M. Tokar, and J. Weiland, *Phys. Plasmas*, **15** 042316 (2008).

[11] T. Fülöp and S. Moradi, *Phys. Plasmas*, **18** 030703 (2011).

[12] J. Candy, R. E. Waltz, *J. Comput. Phys.*, **186** 545 (2003).

[13] L. C. Ingesson, H. Chen, P. Helander and M. J. Mantsinen, *Plasma Phys. Control. Fusion*, **42** 161 (2000).

[14] K. D. Marr, B. Lipschultz, P. J. Catto, R. M. McDermott, M. L. Reinke, A. N. Simakov, *Plasma Phys. and Control. Fusion*, **52** 055010 (2010).
[15] I. Condrea, E. Haddad, C. Cote and B. C. Gregory, *Plasma Phys. Control. Fusion* **43**, 71 (2001).
[16] J. E. Rice, J. L. Terry, E. S. Marmar, F. Bombarda, *Nucl. Fusion*, **37** 241 (1997).
[17] M. Romanelli and M. Ottaviani, *Plasma Phys. Control. Fusion*, **40** 1767 (1998).
[18] T. Sunn Pedersen, R. S. Granetz, E. S. Marmar, D. Mossessian, J. W. Hughes, I. H. Hutchinson, J. Terry, J. E. Rice, *Phys. of Plasmas*, **9** 4188 (2002).
[19] P. Helander, *Phys. of Plasmas*, **5** 3999 (1998).
[20] T. Fülöp, P. Helander, *Phys. of Plasmas*, **6** 3066 (1999).
[21] T. Fülöp, P. Helander, *Phys. of Plasmas*, **8** 3305 (2001).
[22] M. Landreman, T. Fülöp, D. Guszejnov, http://arxiv.org/abs/1104.0597v1, submitted to *Phys. of Plasmas* (2011).
[23] F. Romanelli and S. Briguglio, *Phys. Fluids B*, **2** 754 (1990).
[24] I. Pusztai, T. Fülöp, J. Candy and J. R. Hastie, *Phys. Plasmas*, **16**, 072305 (2009).
[25] T. Fülöp and H. Nordman, *Phys. Plasmas* **16**, 032306 (2009).
[26] C. Angioni, A. G. Peeters, G. Pereverzev, A. Bottino, J. Candy, R. Dux, E. Fable, T. Hein and R. E. Waltz, *Nucl. Fusion* **49** 055013 (2009).
[27] M. E. Puiatti, M. Mattioli, G. Telesca, M. Valisa, I. Coffey, P. Dumortier, C. Giroud, L. C. Ingesson, K. D. Lawson, G. Maddison, A. M. Messiaen, P. Monier-Garbet, A. Murari, M. F. F. Nave, J. Ongena, J. Rapp, J. Strachan, B. Unterberg, M. von Hellermann and contributors to the EFDA-JET Workprogramme, *Plasma Phys. Control. Fusion*, **44** 1863 (2002).
[28] M.F.F. Nave, J. Rapp, T. Bolzonella, R. Dux, M.J. Mantsinen, R. Budny, P. Dumortier, M. von Hellermann, S. Jachmich, H.R. Koslowski, G. Maddison, A. Messiaen, P. Monier-Garbet, J. Ongena, M.E. Puiatti, J. Strachan, G. Telesca, B. Unterberg, M. Valisa, P. de Vries and contributors to the JET-EFDA Workprogramme, *Nucl. Fusion*, **43** 1204 (2003).
[29] O. Gruber, A. C. C. Sips, R. Dux. T. Eich, J. C. Fuchs, A. Herrmann, A. Kallenbach, C. F. Maggi, R. Neu, T. Pütterich, J. Schweinzer, J. Stober and the ASDEX Upgrade team, *Nucl. Fusion* **49**, 115014 (2009).